Computational Organic Chemistry: Examples of Applications.

Alessandro Contini (*)
alessandro.contini@unimi.it

Istituto di Chimica Organica "Alessandro Marchesini", Facoltà di Farmacia, Università degli Studi di Milano, Milano (*)

(Received on July 19, 2006)

Abstract

Grazie al notevole incremento delle prestazioni dei moderni processori e all'ottimizzazione del software per un utilizzo parallelo, l'interesse dei chimici organici verso le tecniche di calcolo quanto–meccanico è notevolmente aumentato. La chimica quantistica permette infatti di calcolare a priori numerose proprietà molecolari (per esempio energia, geometria favorita, proprietà spettroscopiche) e di rendere possibile studi meccanicistici tramite l'analisi accurata degli stati di transizione. In questo articolo vengono presentati due esempi dove le tecniche di calcolo quantomeccanico si sono rivelate utili per risolvere problemi interpretativi sorti durante alcune attività di ricerca sperimentale nel campo della chimica organica. Nel primo caso, il fenomeno della tautomeria di derivati imidazolici è stato studiato tramite il confronto delle loro caratteristiche spettroscopiche derivate sperimentalmente con quelle calcolate per i singoli tautomeri. Nel secondo esempio il calcolo quantomeccanico ha permesso di razionalizzare la duplice reattività degli o-thiochinoni nelle cicloaddizioni di Diels–Alder. Gli studi computazionali descritti nel presente articolo sono stati resi possibili grazie alla collaborazione tra l'Università degli Studi di Milano e il CILEA, che ha messo a disposizione i propri supercalcolatori.

The interest of the organic chemists toward computational quantum mechanics (QM) is notably grown due to both the increasing performance of modern CPU's and the software optimization for parallel applications. Indeed, quantum chemistry allows the prediction of several molecular properties (i.e. energy, favored geometry, spectroscopic properties) as well as the investigation of reaction mechanisms trough an accurate analysis of transition states (TS). In this manuscript we report two examples where quantum–chemical computational techniques were successfully applied to solve some questions raised within research

projects in the field of organic chemistry. The first example concerns the study of the tautomerism (a phenomenon of dynamic chemical equilibrium) of some imidazole derivatives, where their experimentally derived spectroscopic properties were compared with those theoretically computed for the single tautomers. In the second case, computational QM allowed the rationalization of the "double-faced" reactivity of o-thioquinones toward Diels–Alder cycloadditions. The studies herein reported were performed thanks to the collaboration between the Università degli Studi di Milano and CILEA, which provided computational facilities.

Keywords: Quantum–chemical calculations, tautomerism, Diels–Alder

Introduction

Researchers in the field of organic chemistry have often to deal with problems that are not easily solvable by standard experimental techniques. For example, transition state theory is often invoked to rationalise those chemical processes which lead to more than one product, but transition states are not observable by current analytical instruments. However, since the beginning of the last century, quantum chemists and physicists discovered rules allowing the description of molecules, and thus their properties, by mathematical equations. Such equations are rather complex to solve and only the development of powerful and fairly easy to use computers, together with software packages, actually allowed the theoretical study of reasonably sized molecular systems. Computational chemistry allows a fast and extremely accurate calculation of molecular features such as the geometrical arrangement of the nuclei that corresponds to stable molecules or transition states, their energies and their properties such as dipole moment, IR frequencies, NMR shieldings, optical activity, and more [1]. It is thus evident that computational chemistry represents an invaluable tool in the hands of organic chemists for the design of efficient processes, the interpretation of unexpected results or the analytical characterization of novel molecular systems. The following examples, taken from the extensive work reported in references [2] and [3], respectively, describe how quantum chemical calculations resulted essential in order to achieve a thorough understanding of the investigated chemical questions.

Tautomerism of Coumarin Condensed Imidazoles. Coumarin condensed imidazoles **1a–e** (Figure 1) could virtually exist in four tautomeric forms, namely N3–H, N1–H, coumarin O–H and C2–H (α, β, γ and δ tautomer, respectively).

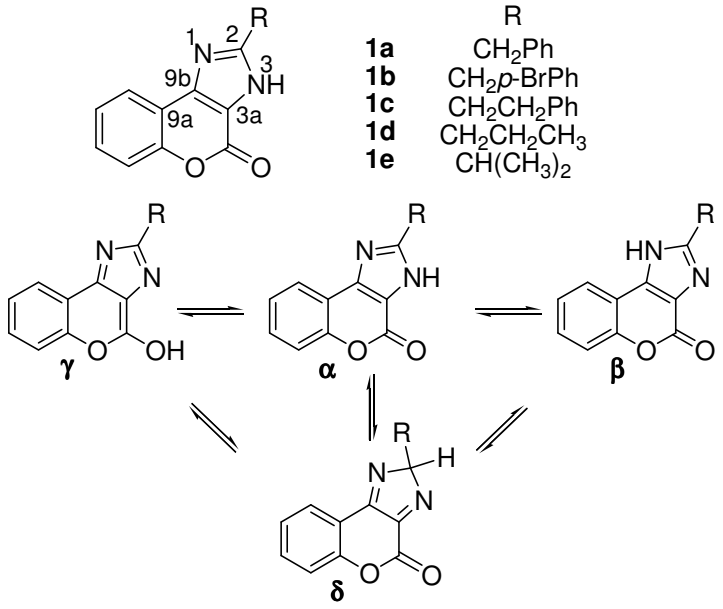

Figure 1. Possible tautomers of compounds **1a–e**.

Experimental evidences reported so far were unable to lead to an unique statement about the preferred tautomeric forms in solution [4]. Thus, aiming to clarify the tautomeric equilibrium of such compounds, the relative stability of the possible tautomers for **1a-e** was evaluated by mean of B3LYP/TZVP//B3LYP/6-31G** calculations [5], including the solvent contribution (acetone and DMSO) by the SCRF CPCM model [6].

Table1. Relative enthalpies (kcal/mol) for α, ß, γ and δ tautomers of compounds **1a-e** together with dipole moments μ (in Debyes) and percent population of α and ß, calculated in Gas Phase or in DMSO.

		ΔH				μ		pop% [a]	
cmpd	Medium	α	β	γ	δ	α	β	α	β
1a	Gas	0.0	4.4	23.1	30.9	3.68	8.39		
	Phase							99.9	0.1
	DMSO	0.0	0.7	22.6	30.8	4.34	12.05	77.0	23.0
1b	Gas	0.0	4.3	22.0	30.2	3.62	6.95		
	Phase							99.9	0.1
	DMSO	0.0	0.7	22.7	31.4	4.80	10.31	76.3	23.7
1c	Gas	0.0	4.0	22.2	32.2	3.70	8.61		
	Phase							99.9	0.1
	DMSO	0.0	1.3	21.4	32.2	4.54	11.94	90.2	9.8

1d	Gas	0.0	4.7	21.7	30.7	3.72	8.18		
	Phase							100.0	0.0
	DMSO	0.0	0.2	23.9	34.2	4.47	12.28	57.0	39.1
1e	Gas	0.0	4.9	21.8	30.4	3.66	7.97		
	Phase							100.0	0.0
	DMSO	0.0	0.1	24.2	33.4	4.48	12.18	56.0	44.0

[a] Calculated accordingly to the Boltzmann's equation at T=298 K.

The first evidence was that the α and the ß forms are the only relevant tautomers of compounds **1a–e** both in vacuum and in solution. This result was actually expected, as the IR spectra exhibited only the typical lactone bands at 1704–1712 cm^{-1} whereas the OH stretching at 3000–3500 cm^{-1}, indicative for the γ tautomer, was never detected. On the other hand, the δ form was never observed on the basis of ^{1}H and ^{13}C-NMR spectra, and those experimental results gave strength to our methodological choice for theoretical calculations. Concerning the two N–H tautomers, the vacuum preferred form is decidedly the α tautomer which resulted more stable than ß from 4.0 to 4.9 kcal/mol, as observed for compounds **1c** and **1e**, respectively. Thus, accordingly to the Boltzmann's equation, the calculated population of the α tautomer in the gas phase and in standard conditions resulted more than 99% for all the investigated compounds. However, the introduction of the solvent contribution gave rise to a drop of the α–ß energy difference and the relative enthalpies resulted between 0.1 and 1.3 kcal/mol in DMSO as observed for **1e** and **1c**, respectively. The stabilization of the ß tautomer in DMSO is not surprising taking into account its higher dipole moment μ, compared to the α form, and thus its higher affinity for the polar solvation medium. Energy values reported in Table 1 show that the α–ß tautomeric equilibrium is possible for all the investigated compounds, however energetic differences between the α and ß tautomer are very close to the accuracy limit expected for the computational methods employed. Moreover, it should be considered that RT NMR experiments performed so far generally showed a unique compound. This can be due to the fact that the α tautomer, being the most stable, is the only detectable form in solution. Otherwise both the α and ß tautomers can be simultaneously present, even if at different concentrations, but their equilibrium rate is faster than the NMR timescale and thus only an averaged spectrum can be recorded. For the above reasons, ^{13}C absolute shielding σ were computed using the GIAO method [7] at the B3LYP/TZVP//B3LYP/6-31G** level for the α and ß tautomeric forms of compounds **1a–e** and then converted in chemical shifts δ for a better correlation with experiments.

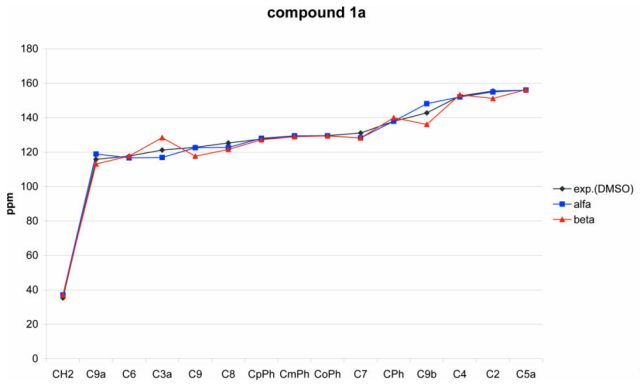

Figure 2. Experimental vs. theoretical ^{13}C chemical shifts for compound **1a**

Table 2. Correlation between experimental (DMSO-d6) and theoretical ^{13}C chemical shifts for compounds **1a–e**, together with the quadratic sum of all deviations [a] and the relative population calculated for α and β tautomers.[b]

	1a		**1b**		**1c**		**1d**		**1e**	
	α	β	α	β	α	β	α	β	α	β
R^2	0.993	0.986	0.960	0.948	0.997	0.991	0.998	0.991	0.997	0.987
$\Sigma\Delta\delta^2$	68.5	128.7	420.5	469.9	110.0	192.1	359.8	861.6	339.6	491.2
Pop%	65.3	34.7	52.8	47.2	63.6	36.4	70.5	29.5	59.1	40.9

[a] Deviations $\Delta\delta\%$ are evaluated as $\Delta\delta\% = 100(\delta_{calc}-\delta_{exp})/\delta_{exp}$; $\Sigma\Delta\delta^2$ is the quadratic sum of all deviations $\Delta\delta\%$. [b] Calculated as $Pop\%_{\alpha\beta} = 100[\Sigma\Delta\delta^2{}_{\beta\alpha} / (\Sigma\Delta\delta^2{}_{\alpha} + \Sigma\Delta\delta^2{}_{\beta})]$.

As depicted in Figure 2 for compound **1a**, the obtained fit between theoretical and experimental values is very good, particularly in the region above 100 ppm where the deviations are generally lower than 1%. Substantially higher deviations were found for those carbons strongly influenced by the tautomeric rearrangement, namely C2, C3a, C9, C9a and C9b, where the experimental value resulted a weighted average of the chemical shifts of the single tautomers. The position of the tautomeric equilibrium was then derived from the quadratic sum of the deviations between the theoretical chemical shifts computed for the single tautomers and the experimental values. Percent populations reported in Table 2 show an α tautomer population of about 70% for compound **1d**, and 53% for compound **1b**. Compounds **1a**, **1c** and **1e** lie in the middle with percent values of 65, 64 and 59%, respectively. A further comparison with experimental results was then desirable in order to determine which of the above described methods provides the most accurate description of the tautomeric equilibrium here investigated. For

this reason dynamic ^{1}H NMR spectra were recorded in acetone at a temperature range from RT to 173 K in order to evidence and quantify all possible tautomers in solution by lowering their conversion rate. The major tautomer population resulted within 58.5 and 69.4% as obtained for compounds **1b** and **1d**, respectively. Compounds **1a** and **1c** provided values close to the upper limit (67,6 and 68.5%, respectively), while compound **1e** showed a major tautomer population of 63.7%. Such values are in particularly good concordance with the percent populations obtained from the comparison of theoretical and experimental ^{13}C chemical shifts (see Table 2), confirming this latter method as the most predictive for the study of tautomeric equilibrium.

Reactivity of o-thioquinones toward 1,3 dienes. Cycloadditions of *o*-thioquinones (*o*-TQs) with 1,3-dienes could proceed via either a [2+4] or a [4+2] mechanism, as depicted in Figure 3 for the reaction of *o*-TQ **2a** with diene **3c** [8].

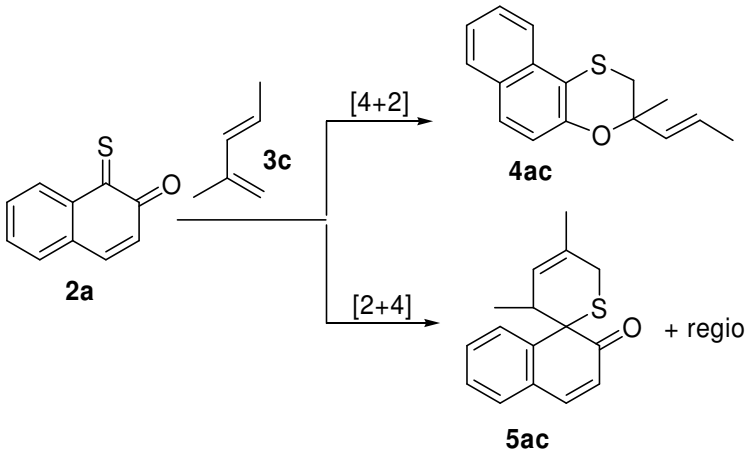

Figure 3. Possible reaction paths for the cycloaddition of *o*-TQs **2** and 1,3–dienes.

The computational study hereafter described is based upon the optimization of 9 reactants (3 *o*-TQs and 6 1,3-dienes), 62 products and 86 different transition structures, corresponding to the approaches of *o*-TQs to 1,3-dienes for both the [4+2] and [2+4] reaction paths, including TSs leading to allowed but not experimentally observed products and/or regioisomers, together with *endo* and *exo* TSs that, due to the symmetric nature of some of the dienes would lead to the same product. However, for reasons of clarity only the model reaction of **2a** with **3c** will be herein described. Computed activation barriers showed that the [2+4] reaction path is kinetically favored. Indeed the activation enthalpies for the [2+4] path resulted lower than those observed for the corresponding [4+2] paths. Instead, [4+2] reactions resulted decidedly favored by the thermodynamic point of view as, in terms of reaction enthalpies ΔH, oxathiin derivative **4ac** is more stable than the spiro derivative **5ac**. Such results fit perfectly with the reported experimental outcome of

[4+2] and [2+4] cycloadditions of *o*–TQs. The reaction mechanism was then thoroughly analysed, and *endo*/*exo* preferences for both reaction paths were investigated. The energetic values obtained for the *endo* and *exo* TSs for [2+4] and [4+2] reactions show that for the [4+2] cycloaddition the *endo* approach is favored, while for the [2+4] reaction the *exo* approach is decidedly preferred. Those results were confirmed by performing extensive IRC analyses starting from the *endo* or *exo* TSs for both [2+4] and [4+2] reactions. IRC results are depicted graphically in Figure 4.

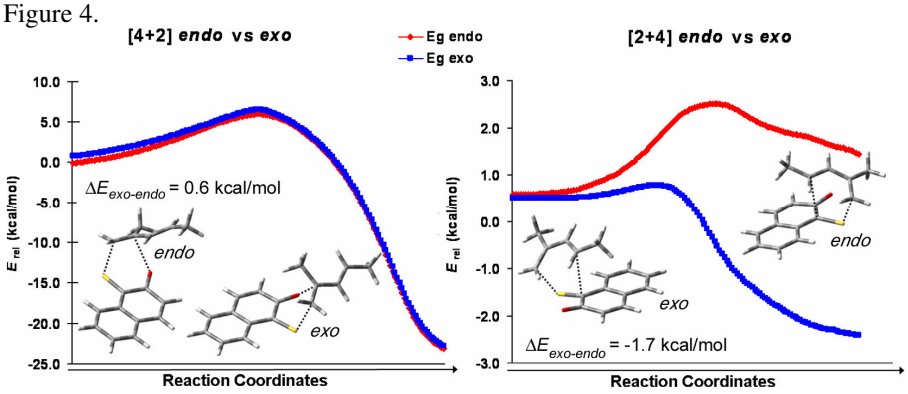

Figure 4. B3LYP/6-31G* IRC analyses of the endo and exo approaches for the [4+2] and [2+4] cycloadditions of o-TQ **2a** with diene **3c**.

Analyzing the reaction mechanism, it was observed that the [4+2] cycloaddition takes place in a quite asynchronous manner, but only one TS was located, suggesting that the mechanism is fully concerted. On the other hand, the geometrical parameters for the [2+4] TS show that the reaction takes place in an unconcerted manner. Indeed, two separate TSs, one for the formation of the C–S bond (**TS–5ac**, IF=-108.734 cm^{-1}), the other for the formation of the C–C bond (**TS2–5ac**, IF=-123.688 cm^{-1}), and the stable intermediate **I–5ac** were located over the [2+4] potential energy surface (PES), thus supporting a stepwise mechanism for this example reaction. In order to exclude any solvent influence on such two–step mechanism, reactants, TSs, the intermediate and product were reoptimized at the B3LYP/6-31G* level including the solvent contribution ($CHCl_3$) by mean of the PCM model [9], but analogue stationary points were located along the PES. Finally, the regioselectivity of [4+2] and [2+4] reactions was analyzed in terms of both FMO theory and reaction PES.

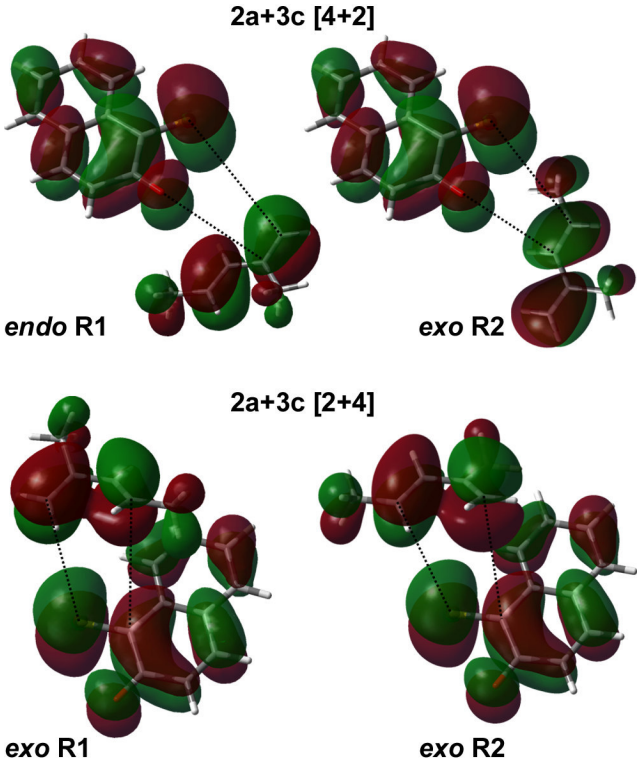

FIGURE 6. Symmetry allowed $LUMO_{o\text{-}TQ}$–$HOMO_{1,3\text{-}diene}$ interactions for [4+2] and [2+4] paths.

HOMO and LUMO energies show that both the [4+2] and [2+4] cycloadditions are controlled by the interaction of the LUMO of the *o*-TQs with the HOMO of the 1,3-diene. Thus, the [4+2] cycloaddition follows an inverse electron–demand pathway while the [2+4] reaction formally follows a direct electron–demand pathway as in [2+4] the *o*-TQ act as the dienophile. As depicted in Figure 6, the shape and the sign of the frontier molecular orbitals involved in the reaction show that both [4+2] and [2+4] cycloadditions could virtually provide two symmetry allowed regioisomers, namely R1 and R2. The [4+2] R1 and R2 isomers derive from the energetically favored and symmetry allowed *endo*- and *exo*-TSs, respectively, while for both the [2+4] R1 and R2 isomers the *exo*-TSs resulted decidedly favored. Concerning the [4+2] reaction the R1 regioisomer is both kinetically and thermodynamically favored and thus, in perfect concordance with experimental results, R1 is the only expected regioisomer. Concerning the [2+4] reaction, the available experimental results show that the products were obtained as a mixture of R1 and R2 regioisomers. Activation enthalpies show that the R1 isomer is kinetically favored ($\Delta\Delta H^{\ddagger}_{R2-R1}$=2.1 kcal/mol) while reaction enthalpies ΔH show

that the R2 regioisomer is thermodynamically favored, as $\Delta\Delta H_{R2\text{-}R1}$ values resulted -4.1 kcal/mol. Thus, the competitive kinetic and thermodynamic pathways suggest that [2+4] reactions of *o*-TQs with asymmetric dienes would lead to mixtures of regioisomers, in concordance with the qualitative predictions based on the FMO theory (see Figure 6) as well as with the available experimental results.

References

[1] F. Jensen, *Introduction to Computational Chemitry*, John Wiley & Sons Ltd, 2001.

[2] A. Contini, D. Nava, P. Trimarco *J. Org. Chem.* 2006

[3] A. Contini, S. Leone, S. Menichetti, C. Viglianisi, P. Trimarco *J. Org. Chem.* 2006

[4] E. Beccalli, A. Contini, P. Trimarco *Eur. J. Org. Chem.* 2003 and ref. cited therein.

[5] A. D. Becke *J. Chem. Phys.*, 98, 5648-5652, 1993.

[6] F. Eckert, A. Klamt *AIChE J.*, 48, 369-385, 2002.

[7] Wolinski, K.; Hinton, J. F.; Pulay, P., *J. Am. Chem. Soc.*, *112*, 8251-8260, 1990.

[8] Menichetti, S.; Viglianisi, C. *Tetrahedron*, *59*, 5523–5530, 2003.

[9] Cammi, R.; Mennucci, B.; Tomasi, J. *J. Phys. Chem. A*, *104*, 5631–5637, 2000.

[10] Gaussian 03, Revision B.04, M. J. Frisch et al., Gaussian, Inc., Pittsburgh PA, 2003.

Acknowledgments

All calculations herein described were performed with the Gaussian03 package [10] installed on the 256 CPU cluster (Avogadro) hosted by the "Centro Interuniversitario Lombardo per l'Elaborazione Automatica" (CILEA) Segrate MI. Thus we would like to thank all the staff at CILEA for the support in installing, configuring and running the software packages requested for our research projects.